Chemical Geology 250 (2008) 68–78

Contents lists available at ScienceDirect

Chemical Geology

journal homepage: www.elsevier.com/locate/chemgeo

H_2O diffusion models in rhyolitic melt with new high pressure data

Huaiwei Ni, Youxue Zhang *

Department of Geological Sciences, The University of Michigan, 2534 C. C. Little Bldg., 1100 North University Ave., Ann Arbor, MI 48109-1005, USA

ARTICLE INFO

Article history:
Received 20 June 2007
Received in revised form 5 January 2008
Accepted 11 February 2008

Editor: D. Rickard

Keywords:
H_2O diffusion
Bubble growth
Rhyolite
Volcanic eruptions
Diffusivity model
Pressure effect

ABSTRACT

Water diffusion in silicate melts is important for understanding bubble growth in magma, magma degassing and eruption dynamics of volcanos. Previous studies have made significant progress on water diffusion in silicate melts, especially rhyolitic melt. However, the pressure dependence of H_2O diffusion is not constrained satisfactorily. We investigated H_2O diffusion in rhyolitic melt at 0.95–1.9 GPa and 407–1629 °C, and 0.2–5.2 wt.% total water (H_2O_t) content with the diffusion-couple method in a piston-cylinder apparatus. Compared to previous data at 0.1–500 MPa, H_2O diffusivity is smaller at higher pressures, indicating a negative pressure effect. This pressure effect is more pronounced at low temperatures. Assuming H_2O diffusion in rhyolitic melt is controlled by the mobility of molecular H_2O (H_2O_m), the diffusivity of H_2O_m (D_{H_2Om}) at $H_2O_t \leq 7.7$ wt.%, 403–1629 °C, and ≤1.9 GPa is given by

$$D_{H_2O_m} = D_0 \exp(aX),$$

$$\text{with } D_0 = \exp\left(13.375 + 1.8875P - \frac{12939 + 3625.6P}{T}\right),$$

$$\text{and } a = -37.256 + \frac{75884}{T},$$

where D_0 is in $\mu m^2/s$, X is mole fraction of H_2O_t on a single oxygen basis, T is temperature in K, and P is pressure in GPa.

H_2O_t diffusivities (D_{H_2Ot}, in $\mu m^2/s$) can be calculated from H_2O_m diffusivity, or directly from the following expression:

$$\ln\left(D_{H_2O_t}/X\right) = 13.47 - 49.996X + 7.0827\sqrt{X} + 1.8875P - \frac{9532.3 - 91933X + 13403\sqrt{X} + 3625.6P}{T}.$$

At low H_2O_t content (up to 2 wt.% if an error of a factor of 2 is allowed), H_2O_t diffusivity is approximately proportional to H_2O_t content:

$$D_{H_2O_t} = \frac{C}{C_0}\exp\left(9.5279 + 1.8875P - \frac{9698.5 + 3625.6P}{T}\right),$$

where C is H_2O_t content in wt.% and C_0 is 1 wt.%. The new expressions for H_2O diffusion not only reproduce our own data, but also match data in literature from different laboratories and using different methods, indicating good inter-laboratory and multi-method consistency. The new expressions cover a wide range of geological conditions, and can be applied to H_2O diffusion in rhyolitic melts in various volcanic and magmatic processes.

1. Introduction

Water is a major volatile component in natural silicate melts. The diffusion of water is necessary to the understanding of a series of volcanic processes, such as bubble growth (e.g., Liu and Zhang, 2000),

* Corresponding author. Tel.: +1 734 763 0947; fax: +1 734 763 4690.
E-mail address: youxue@umich.edu (Y. Zhang).

0009-2541/$ – see front matter © 2008 Elsevier B.V. All rights reserved.
doi:10.1016/j.chemgeo.2008.02.011

magma degassing, and magma fragmentation (Zhang, 1999a). Within natural melts, rhyolite has been the most thoroughly investigated with respect to H_2O diffusion due to common occurrences of explosive rhyolitic eruptions. Early workers used measurements involving bulk hydration/dehydration (Shaw, 1974; Friedman and Long, 1976; Jambon, 1979) or the ion microprobe (Delaney and Karsten, 1981; Karsten et al., 1982; Lapham et al., 1984). They demonstrated H_2O diffusivity in rhyolitic melt increases with its concentration. Infrared and NMR studies (e.g., Orlova, 1962; Bartholomew and Schreurs, 1980; Stolper, 1982) showed that water is present in silicate melts as at least two species: molecular H_2O (H_2O_m) and hydroxyl group (OH). Therefore, in order to understand the fundamental mechanism of H_2O diffusion in melts, it is instructive to understand the role of water speciation in diffusion (Wasserburg, 1988).

Zhang et al. (1991) investigated the dehydration of rhyolite samples with total H_2O content (H_2O_t) <2 wt.% at low temperatures (403–530 °C), which allows the concentrations of the two H_2O species preserved through quenching for infrared determination (Zhang et al., 1995, 1997a; Withers et al., 1999). They concluded that H_2O_m is the dominant diffusing species, whereas OH is almost immobile and its concentration profile is due to species conversion to maintain equilibrium. Furthermore, they assumed concentration-independent H_2O_m diffusivity and modeled the concentration profiles well. Later, it was found that the concentration-independent H_2O_m diffusivity assumption of Zhang et al. (1991) cannot be extended to high H_2O content (up to 9.1 wt.%) (Behrens and Nowak, 1997; Nowak and Behrens, 1997). Zhang and Behrens (2000) proposed that H_2O_m diffusivity increases exponentially with H_2O_t and successfully reconciled all the experimental data covering a fairly wide range of temperature (403–1215 °C), pressure (0.1–810 MPa) and water content (0.1–7.7 wt.%). [The exponential dependence of the diffusivity of a neutral molecular or atomic species has also been observed for CO_2 (Watson, 1991) and Ar (Behrens and Zhang, 2001).] Okumura and Nakashima (2004) reported new H_2O diffusion data using *in situ* measurements of dehydration experiments. Behrens et al. (2007) investigated both H_2O and ^{18}O diffusion at 100 MPa from hydration experiments, demonstrating H_2O_m is the carrier of ^{18}O diffusion. Other natural melts that have been investigated for H_2O diffusion include basalt (Zhang and Stolper, 1991; Okumura and Nakashima, 2006), andesite (Behrens et al., 2004, Okumura and Nakashima, 2006), dacite (Behrens et al., 2004, Liu et al., 2004, Okumura and Nakashima, 2006), and trachyte (Freda et al., 2003).

This study focuses on H_2O diffusion in rhyolitic melt. Although H_2O diffusion in rhyolite has been investigated extensively, the pressure dependence of H_2O diffusivity has not been well resolved, compared to temperature and water concentration dependence, as pointed out by Zhang and Behrens (2000) and Zhang et al. (2007). The majority of the experiments that constrained the dependence of diffusivity on H_2O content in Zhang and Behrens (2000) were at 500 MPa. Therefore, application of their model to pressures other than 500 MPa may not be accurate. Behrens et al. (2007) noted that the dependence of H_2O diffusivity on H_2O content at 100 MPa differs from that predicted by Zhang and Behrens (2000). Because volcanic eruption is a decompressional process as the magma is upwelling, the pressure effect on H_2O diffusivity is crucial and needs to be evaluated more accurately. To fulfill such a need, we carried out an experimental investigation on H_2O diffusion at 0.95–1.9 GPa and 407–1629 °C, so that the pressure range (0–1.9 GPa) is large enough to constrain the pressure effect and to infer H_2O diffusivity at <0.5 GPa for modeling bubble growth and volcanic degassing. (Diffusion experiments at low pressure such as 0.1 MPa and high H_2O_t content cannot be accomplished because of bubble formation.) Our study makes the rhyolitic system the first for which H_2O diffusivity is known as a function of temperature (400–1630 °C), pressure (0–2 GPa) and H_2O content (0–8 wt.%).

2. Experimental and analytical methods

2.1. Starting materials

One of the starting materials, the anhydrous rhyolitic glass CIT, is a natural sample from Coso Range, California (Newman et al., 1986), containing small amounts of microlites and bubbles. These imperfections are not expected to have much effect on H_2O diffusion. The water content is 0.20–0.22 wt.%. Hydrous rhyolitic glasses with H_2O_t content of 4 to 5 wt.% are synthesized by loading dry glass powder and water into $Au_{80}Pd_{20}$ capsules in alternating portions and heated at 1000 °C and 500 MPa for 3 days in an internally heated pressure vessel (IHPV) at the University of Hannover. Sample GMR+2 is synthesized at 1400 °C overnight from dry rhyolitic glass from Glass Mountain, California (Hui et al., 2008a). These rapidly quenched (initially 200 °C/min under isobaric conditions) hydrated samples are transparent and free of crystals and bubbles, and contain 2.3 wt.%, 4.0 wt.%, and 5.2 wt.% H_2O_t homogeneously distributed (<3% relative variability). All anhydrous and hydrous rhyolite glasses are light brown in color, and are analyzed with a Cameca SX100 electron microprobe at the University of Michigan. The dry compositions of all rhyolite samples used in this study are similar, as reported in Table 1, except for a slightly lower silica content for GMR-2. No significant differences in H_2O diffusivity between GMR-2 and other samples were noticed. Anhydrous rhyolite cylinders of 1.2–1.5 mm thickness, and hydrous cylinders of 2.5–2.9 mm thickness were prepared and doubly polished for infrared analysis and subsequent diffusion-couple experiments.

2.2. Diffusion-couple experiments

Diffusion-couple experiments were carried out in a 0.5″ end-loaded piston–cylinder apparatus at the University of Michigan. Anhydrous and hydrous rhyolitic glass cylinders of the same diameter (~2.4 mm) were placed into a platinum tube that was welded shut. The less dense hydrous half was always on top of the anhydrous half to mitigate convection. Crushable MgO rod and a $BaCO_3$ cell were used as pressure medium inside and outside the graphite furnace, respectively.

The experimental temperature was monitored by a type D thermocouple (Re_3W_{97}–$Re_{25}W_{75}$) and simultaneously recorded by a computer program. In high temperature runs (1118–1629 °C), water diffusion is rapid and only a short duration (2–10 min) is necessary. Therefore, a stepwise heating procedure was programmed with a Eurotherm controller so that it took only ~24 s from the relaxation temperature (200 °C) to the target temperature with only small overheating of 1–4 °C. Because the experimental durations of low

Table 1
Composition of rhyolitic glasses (wt.% on anhydrous basis)

	CIT	GMR+2	Rhy4	Rhy5
SiO_2	76.93	73.12	76.87	76.05
TiO_2	0.05	0.28	0.04	0.10
Al_2O_3	13.18	14.49	13.38	13.93
FeO_T	0.94	1.35	0.97	0.75
MnO	0.04	0.06	0.04	0.04
MgO	0.02	0.29	0.03	0.12
CaO	0.44	1.30	0.55	0.87
Na_2O	4.29	4.27	4.14	4.01
K_2O	4.62	4.36	4.65	4.22
P_2O_5	0.04	0.09	0.01	0.07
Total	100.55	99.61	100.68	100.16
H_2O (IR)	0.20	2.27	3.96	5.17

For each sample, 5 analyses are averaged. Analyses are made on a Cameca SX100 electron microprobe using a scanning beam of 15 kV voltage and 4 nA current. Raw oxide contents are divided by (1 − *c*/100) so as to normalize to dry composition, where *c* is the water content from infrared analysis in wt.%.

temperature runs (407–609 °C) were relatively long (>24 h), manual heating was applied and it took ~1 min to reach the target temperature from the relaxation temperature of 100 °C. Temperature fluctuation during the experiment was generally within ±1 °C, but spikes of ±5 °C were observed for several brief periods (~5 s) in long experiments. Experimental assemblages were rapidly quenched (with a mean cooling time scale of 8 s based on Zhang et al., 2000) by chilled water after turning off the power. A typical thermal history of high temperature runs, including relaxation, dwelling, and quenching, is plotted in Fig. 1. Effective duration accounting for diffusion during heating and cooling was estimated to be 12–16 s by assuming an activation energy of 100 kJ/mol for water diffusion, based on the method described in Zhang and Behrens (2000). Adjustment of about 20 s (including the effect of temperature spikes) for long duration experiments (>24 h) is negligible and not applied. Temperature at the center of the experimental charge is the thermocouple temperature plus a correction based on the calibrated temperature gradient inside the charge (Hui et al., 2008a). The overall uncertainty in temperature is estimated to be 10 K.

The pressure is manually kept at either 1 or 2 GPa using a piston-out procedure. Based on our pressure calibration on this piston–cylinder apparatus, the real pressure is roughly 5% lower than nominal pressure based on quartz–coesite transition against the phase boundary determined by Bose and Ganguly (1995). A similar calibration was carried out on another piston–cylinder apparatus in our lab by Hui et al. (2008a), and the correction is 6%. More details about the pressure calibration can be found in Hui et al. (2008a). Uncertainty associated with pressure is ~50 MPa.

At about 2 GPa, the hydrous rhyolite, especially those having high water content, readily crystallizes when the temperature is above 480 °C, and the liquidus of dry rhyolite increases with pressure. These considerations significantly limit the experimental temperature range. Details of eight successful experiments can be found in Table 2. Six other runs are deemed unsuccessful and not reported because of partial to complete crystallization of the hydrous half, or poor contact between the two halves.

2.3. Infrared analysis

Water contents of starting samples were measured with Fourier transform infrared (FTIR) spectrometry, in the dry and N_2-purged main chamber of the FTIR (Perkin-Elmer Spectrum GX) at the University of Michigan. Doubly polished rhyolite cylinders were attached to a sample holder with pinhole of 531 μm diameter. A NIR source, CaF_2 beamsplitter, and liquid nitrogen cooled InSb detector were used for 64 scans from 9000 to 2000 cm^{-1}.

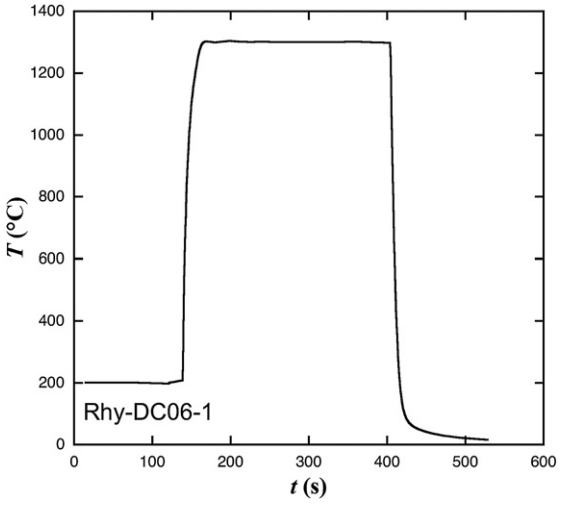

Fig. 1. Thermal history of experiment Rhy-DC06-1, starting from stress relaxation at 200 °C and ending with quenching. The effect of heating up and quenching down on diffusion is equivalent to an extra 13 s at the experimental temperature.

Table 2
Conditions of diffusion-couple experiments

Run #	T (°C)[a]	P (GPa)[b]	Duration (s)[c]	H_2O_t (wt.%) in the two halves	
				Initial	Final
Rhy-DC06-1	1319/1300	1.9/2.0	252/239	4.0/0.2	4.0/0.2
Rhy-DC06-6	1323/1300	1.9/2.0	587/575	2.3/0.2	2.3/0.2
Rhy-DC06-7	1629/1600	1.9/2.0	128/112	5.2/0.2	5.2/0.2
Rhy-DC06-8	609/600	1.9/2.0	86 400	2.3/0.2	2.5/0.2
Rhy-DC06-9	407/400	1.9/2.0	720 000	5.2/0.2	5.3/0.2
Rhy-DC06-11	1118/1100	1.9/2.0	624/611	5.1/0.2	5.1/0.2
Rhy-DC07-12	1321/1300	0.95/1.0	248/236	5.1/0.2	5.1/0.2
Rhy-DC07-14	1120/1100	1.9/2.0	613/601	5.1/0.2	5.1/0.2

[a] 1319/1300 means that the nominal temperature of the thermocouple is 1300 °C. 1319 °C is the corrected temperature based on the calibrated temperature profile.
[b] 1.9/2.0 means that the nominal pressure is 2.0 GPa, 1.9 GPa is the corrected pressure based on quartz–coesite transition against the phase boundary determined by Bose and Ganguly (1995). Pressure is manually controlled at ±20 MPa during diffusion runs.
[c] 252/239 means that the nominal duration is 239 s, and the effective duration after considering diffusion during heating up and cooling down is 252 s.

After a diffusion-couple experiment the quenched sample in Pt capsule was mounted into epoxy resin and a doubly polished section of 200–250 μm thickness was prepared along the cylindrical axis for FTIR microscopy. The thinness reduces the refractive divergence of the infrared beam inside the sample, while still affording reasonable absorbance at the same time. After high temperature runs the glasses usually become lighter colored than their pre-annealing counterparts. Cracks roughly parallel to the interface in the experimental charge, presumably due to shrinkage during quenching, are always present and are a major source of difficulty and error for the FTIR measurements. For some wide cracks, distances must be subtracted to smooth the concentration profile across the cracks.

The Autoimage microscope system, with an MCT (mercury cadmium telluride) detector cooled by liquid nitrogen, is attached to the Spectrum GX spectrometer for the analysis of H_2O concentrations along the diffusion profile. The aperture is 20 μm wide and 200 μm long, but an edge response analysis shows that the spatial distribution of the infrared signal is roughly Gaussian with a full width at half maximum (FWHM) under analysis conditions being about 30 μm. That is, the spatial resolution is much worse than 20 μm. This convolution effect is important for short profiles (<200 μm long) but negligible for longer profiles (>500 μm long), and will be treated further in the Discussion.

A complete diffusion profile, typically 40–80 points, was acquired with background updated after every 5–10 points. Spectra were hand-fitted with two straight tangential baselines (TT method of Withers and Behrens, 1999) at 5230 cm^{-1} and 4500 cm^{-1}. Peak heights were measured to calculate molecular H_2O (H_2O_m) and hydroxyl group (OH) concentrations, respectively, using the calibration of Withers and Behrens (1999). The sum of H_2O_m and OH is H_2O_t concentration. Although the calibration of Withers and Behrens (1999) may not be able to retrieve accurate species concentration as that of Zhang et al. (1997b) at relatively low H_2O_t (≤2.7 wt.%), it can be applied to H_2O_t up to 9.2 wt.% and is less time-consuming for processing a large amount of spectra.

3. Experimental results

Details of the eight successful experiments are listed in Table 2. All H_2O_t diffusion profiles are illustrated in Fig. 2. Owing to reactions during quench, H_2O_m and OH concentrations from experiments at >700 °C

(depending on H_2O_t content) do not represent their concentrations under experimental conditions. Therefore, directly measured species concentrations are not used for modeling H_2O diffusion.

Far away from the contact between the two halves in a diffusion couple, flat regions of H_2O_t concentration are achieved for all runs, and the averages agree well with the starting glasses (Table 2). Hence, the diffusive transport of H_2O from the hydrous half to the anhydrous half can be treated as diffusion in an infinite medium. Outside the flat region of the anhydrous and hydrous ends and near the capsule, water concentrations may differ from the initial concentrations, attributed to transport along cylinder walls (Zhang and Behrens, 2000). These measured points are excluded from the final data; they are not shown in Fig. 2 and not used for extracting H_2O diffusivity. Diffusion profiles at high temperatures are usually longer and better resolved than those at lower temperatures. Because H_2O diffusivity depends on water content, the diffusion profiles do not resemble error function curves, and it is necessary to consider the dependence of diffusivity on H_2O concentration when modeling these profiles.

This study significantly expands the P–T conditions of H_2O diffusion in rhyolitic melts. Fig. 3 summarizes the coverage of P–T–H_2O_t conditions including data in this and previous studies. The extensive investigations on a wide range of temperature (400–1630 °C), pressure (0–2 GPa), and H_2O_t (0–8 wt.%) allow the construction of a comprehensive model on H_2O diffusivity in rhyolitic melt, which can be applied to almost all relevant geologic conditions.

4. Discussion

4.1. Modeling diffusion profiles

The equation describing the diffusion of total H_2O (H_2O_t) is as follows:

$$\frac{\partial X}{\partial t} = \frac{\partial}{\partial x}\left(D_{H_2O_t}\frac{\partial X}{\partial x}\right), \tag{1}$$

where X is mole fraction of H_2O_t on a single oxygen basis (Stolper, 1982; Zhang, 1999b) and is calculated as $X = C/18.015/[C/18.015+(100-C)/32.49)]$ with C being H_2O_t content in wt.%, t is time, x is distance, and D_{H_2Ot} is H_2O_t diffusivity which depends on H_2O concentration (and therefore depends on x). A common approach for obtaining the concentration dependence of the diffusivity is to use the Boltzmann–Matano method. This method is independent of presumptions of the relation between diffusivity and concentration, but the precision of this method is not high (Zhang and Behrens, 2000). An alternative approach is to assume a diffusivity concentration relation, and whether such an assumption is reasonable can be judged from the quality of the fitting. Because molecular H_2O (H_2O_m) and hydroxyl (OH) may contribute distinctly to H_2O diffusion, the mechanistic approach to H_2O diffusion is to consider the contribution of the two water species (H_2O_m and OH) separately:

$$\frac{\partial X}{\partial t} = \frac{\partial}{\partial x}\left(D_{H_2O_m}\frac{\partial X_m}{\partial x} + D_{OH}\frac{\partial X_{OH}/2}{\partial x}\right), \tag{2}$$

where D_{H_2Om} and X_m are diffusivity and mole fraction of molecular H_2O, and D_{OH} and X_{OH} are diffusivity and mole fraction of hydroxyl group. Zhang et al. (1991) and Zhang and Behrens (2000) concluded that H_2O_m is the dominating diffusion species, and OH is almost immobile. Then Eq. (2) reduces to

$$\frac{\partial X}{\partial t} = \frac{\partial}{\partial x}\left(D_{H_2O_m}\frac{\partial X_m}{\partial x}\right). \tag{3}$$

If the reaction $H_2O_m + O \rightleftharpoons 2OH$ is in equilibrium, X_m can be determined from X using Eq. (13) in Zhang (1999b). The equilibrium constant was determined by Zhang et al. (1997b). By comparing Eqs. (1) and (3), one can find the relation between D_{H_2Ot} and D_{H_2Om}:

$$D_{H_2O_t} = D_{H_2O_m}\frac{dX_m}{dX}. \tag{4}$$

Zhang and Behrens (2000) proposed that molecular H_2O diffusivity depends exponentially on total H_2O content:

$$D_{H_2O_m} = D_0\exp(aX), \tag{5}$$

where a is a parameter depending on temperature and pressure. They used a trial and error method to estimate the value of a. This model fits all the diffusion profiles well. Furthermore, diffusivity of molecular species such as CO_2 and Ar has been shown to depend on H_2O_t exponentially (Watson, 1991; Behrens and Zhang, 2001).

We will also assume Eq. (5) in treating H_2O diffusion profiles. The program code of Zhang and Behrens (2000) is revised so that the parameter a is determined from the fitting rather than by trial and error. Because of this improvement, the uncertainty on the parameter a can also be evaluated (which was the main purpose of revising the code). Hence, in the new code, a and D_0 are to be determined by fitting the profile, among which a is largely determined by the shape of the diffusion profile, and D_0 largely by the length of the diffusion profile (and the value of a). In the new fitting, the Levenberg–Marquardt algorithm (Press et al., 1992) is adopted to calculate new values of the fitting parameters in each iteration until the sum of the squares of residuals is minimized.

The new fitting procedure was successfully applied to the six diffusion profiles acquired at >1100 °C and all are well fit. Two other profiles (Rhy-DC06-8 and Rhy-DC06-9) are not sufficiently long compared to the spatial resolution of FTIR microscope (~30 μm in terms of FWHM). Hence, they are likely distorted and prolonged by the convolution effect (Ganguly et al., 1988) and cannot be used to extract best-fit a. To maintain consistency and find the errors of the best-fit a values, we also applied the new fitting procedure to the profiles at 250–500 MPa in Zhang and Behrens (2000). All best-fit a values (Table 3) apparently form a linear trend with $1/T$ (Fig. 4A), without much dependence on pressure. A weighted linear regression yields

$$a = (-37.256\pm1.863) + \frac{75884\pm2286}{T}, \tag{6}$$

where T is in K. The above equation differs from the expression of a in Zhang and Behrens (2000), who noticed a dependence of a on pressure with data for a small pressure range. With a larger pressure coverage by combining this study and previous studies, the pressure dependence of a is within experimental uncertainty. With a values from Eq. (6), all diffusion profiles, including those reported in Zhang et al. (1991) and Zhang and Behrens (2000), are refit to find the best D_0.

For the two short profiles (Rhy-DC06-8 and Rhy-DC06-9), the fitting procedures differ from the other profiles, to examine the convolution effect. A convoluted profile is computed from the theoretical profile by assuming a Gaussian distribution of infrared signal with FWHM = 30 μm. The convoluted profile is then used to fit the measured profile. The excellent fitting (Fig. 2) further verifies the effect of convolution. Similar convoluting procedure is also tested on long profiles such as Rhy-DC07-12, and the difference is negligible and therefore not applied.

All fitting results are reported in Table 4. The precision of diffusion-couple experiments are generally better than dehydration experiments. Fits of profiles from this work are plotted as solid curves together with data points in Fig. 2, and they match excellently.

D_0 values (in $\mu m^2/s$) in Table 4 are plotted in Fig. 4B. At a fixed pressure, the temperature dependence follows the Arrhenius relation despite crossing the glass transition. D_0 decreases from

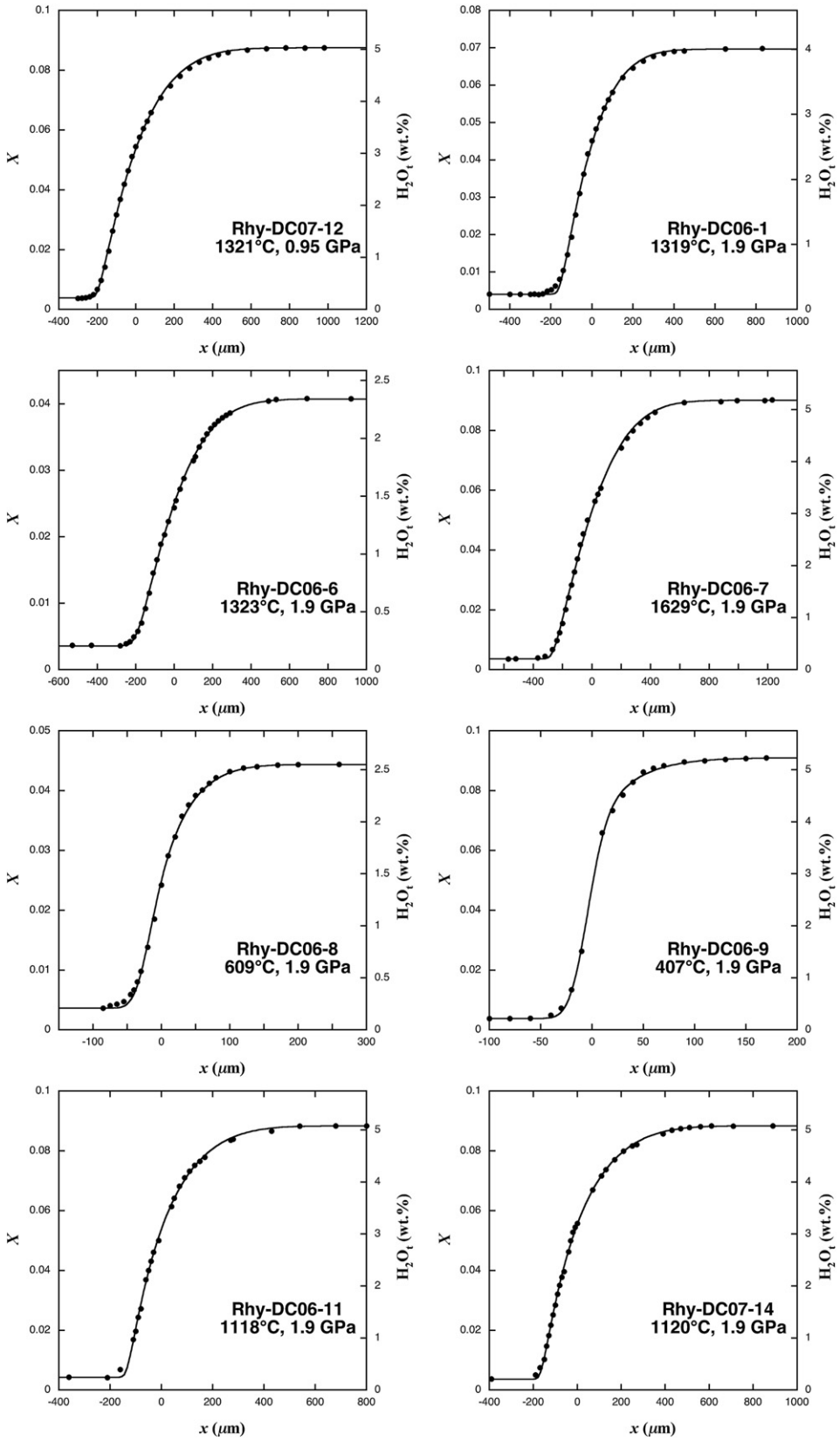

Fig. 2. Diffusion profiles of eight experiments. A crack of 30 μm near the interface is subtracted for Rhy-DC06-9 to smooth the diffusion profile. Solid curves are best fit by Eqs. (5) and (6), with $\ln D_0$ reported in Table 4. Convolution effect is applied for Rhy-DC06-8 and Rhy-DC06-9 (see text). There are data points outside the distance range, which are not shown in order to display the data more clearly.

0.1 MPa to 0.5 GPa to 1.9 GPa, and this negative pressure effect is more pronounced at low temperatures, but becomes minimal at >1200 °C. Hence, at a given pressure, $\ln D_0 = \ln A - E_a/(RT)$, where E_a is the activation energy, R is the gas constant, and A is the pre-exponential factor. When the pressure dependence is examined, not only is the activation energy dependent on pressure, but

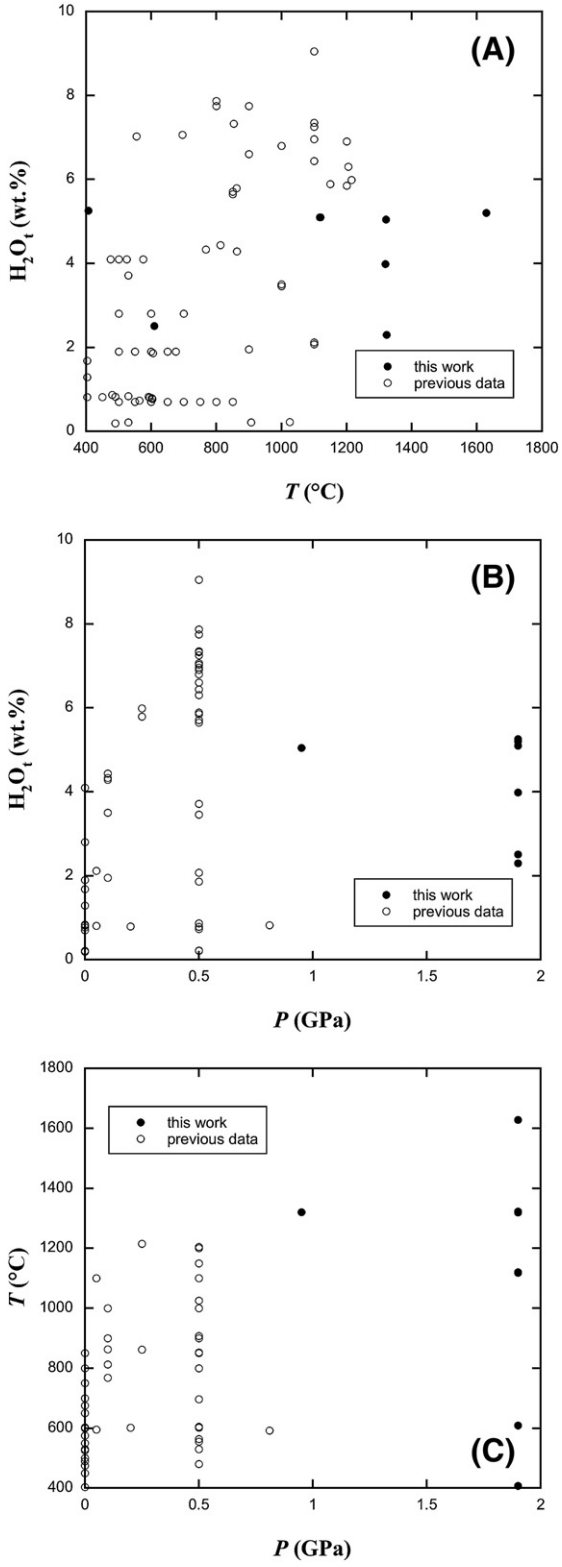

Fig. 3. Coverage of experimental conditions from this work (solid circles) and previous work (open circles) of Zhang et al. (1991), Nowak and Behrens (1997), Zhang and Behrens (2000), Okumura and Nakashima (2004), and Behrens et al. (2007).

also ln$A$. We fit lnD_0 as a function of temperature and pressure as follows:

$$\ln D_0 = (13.375\pm0.483) + (1.8875\pm0.5179)P - \frac{(12939\pm489) + (3625.6\pm647.2)P}{T}. \quad (7)$$

Table 3
Best-fit a values from fitting profiles with the assumption of $D_{H_2Om}=D_0\exp(aX)$

Run #	T (°C)	P (GPa)	t (s)	a	R^2	Source
Rhy-DC07-12	1321	0.95	248	13.53±1.43	0.9998	1
Rhy-DC06-7	1629	1.9	128	6.46±1.86	0.9996	1
Rhy-DC06-6	1323	1.9	587	7.91±3.69	0.9997	1
Rhy-DC06-1	1319	1.9	252	9.04±3.80	0.9994	1
Rhy-DC07-14	1120	1.9	613	16.82±1.88	0.9996	1
Rhy-DC06-11	1118	1.9	624	17.74±3.07	0.9993	1
Rhy-DC1	900	0.5	120	31.76±8.49	0.9978	2
Rhy-DC3	696	0.5	720	39.42±4.99	0.9978	2
Rhy-DC4	853	0.5	240	32.18±4.79	0.9961	2
Rhy-DC5a	555	0.5	9090	55.35±0.58	0.9991	2
Rhy-DC9	1205	0.5	1060	17.48±1.15	0.9998	2
KS&3-D16P	530	0.5	68 520	60.24±7.30	0.9959	2
Rhy-DC10	862	0.25	1920	24.96±2.01	0.9985	2
Rhy-DC11	1215	0.25	1360	7.07±1.19	0.9993	2

Errors of parameter a are given at 2σ level. Source of data: (1)=this work; (2)=refit of data in Zhang and Behrens (2000).

where D_0 is in μm^2/s, T is in K, and P is in GPa. Eq. (7) reproduces all lnD_0 data with a 2σ error of 0.49 and a maximum error of 0.63. If we were to fit lnD_0 without the extra pressure term (the dependence of

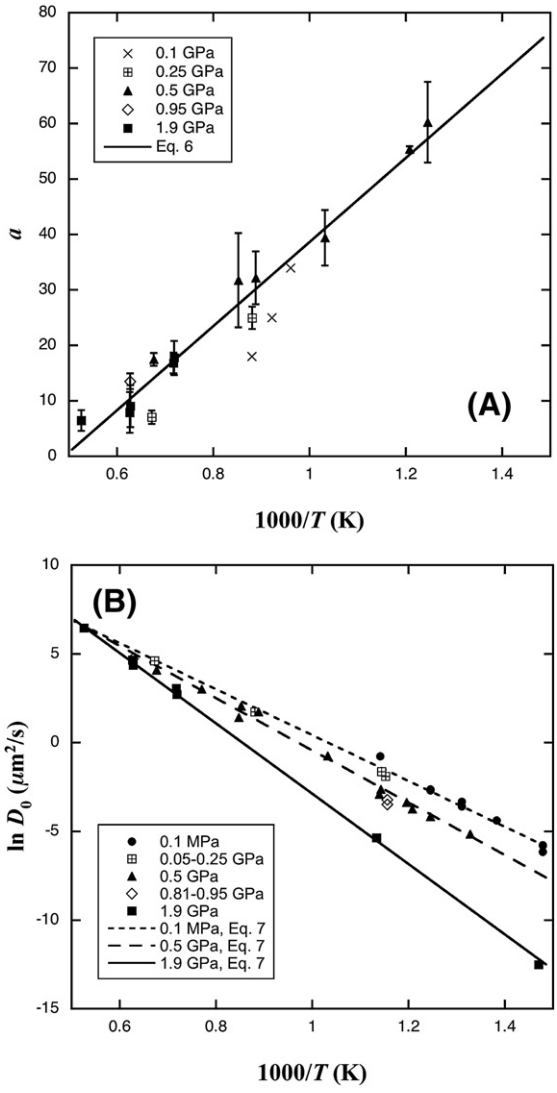

Fig. 4. (A) Best-fit a values (Table 3) from experiments of this work at 0.95–1.9 GPa and those of Zhang and Behrens (2000) at 0.25–0.5 GPa. The straight line is from Eq. (6). Three values at 0.1 GPa from Behrens et al. (2007) are also shown for comparison. (B) Best-fit lnD_0 values reported in Table 4. Straight lines are from Eq. (7).

Table 4
Least-squares fitting results

Run #	T (°C)	P (MPa)	H_2O_t (wt.%)	$\ln D_0$ ($\mu m^2/s$)	R^2	Source
Dehydration experiments						
KS-D2	530	0.1	0.84	−2.69±0.21	0.9884	1
PD-D5	530	0.1	0.22	−2.62±0.15	0.9887	1
KS-D3	490	0.1	0.82	−3.59±0.10	0.9944	1
PD-D4	490	0.1	0.19	−3.33±0.23	0.9890	1
KS-D5A	450	0.1	0.82	−4.38±0.15	0.9889	1
3b-D4N	403	0.1	1.68	−5.78±0.15	0.9927	1
3b-D4	403	0.1	1.29	−5.80±0.08	0.9969	1
KS-D4A	403	0.1	0.81	−6.15±0.23	0.9866	1
KS-D14	603	0.1	0.77	−0.77±0.18	0.9778	2
KS-D13P	595	50	0.81	−1.90±0.09	0.9933	2
KS-D19P	601	200	0.79	−1.63±0.14	0.9822	2
KS-D18P.1	592	810	0.81	−3.22±0.10	0.9866	2
KS-D18P.2	592	810	0.83	−3.47±0.21	0.9782	2
KS-D12P	602	500	0.79	−2.63±0.08	0.9977	2
KS-D23P	563	500	0.74	−3.36±0.14	0.9884	2
KS-D24P	480	500	0.86	−5.15±0.11	0.9939	2
Rhy-D12P	605	500	1.86	−2.91±0.07	0.9979	2
SRhy-DAr1	907	500	0.21	1.43±0.19	0.9831	2
SRhy-DAr2	1025	500	0.22	3.02±0.10	0.9956	2
KS&3-D16P	530	500	3.72	−4.17±0.07	0.9958	2
Diffusion-couple experiments						
Rhy-DC1	900	500	7.7/0.1	2.05±0.12	0.9975	2
Rhy-DC3	696	500	7.1/0.2	−0.73±0.11	0.9975	2
Rhy-DC4	853	500	7.3/0.2	1.75±0.11	0.9960	2
Rhy-DC5a	555	500	7.0/0.1	−3.75±0.09	0.9984	2
Rhy-DC9	1205	500	6.3/0.2	4.09±0.04	0.9996	2
Rhy-DC10	862	250	5.8/0.1	1.74±0.06	0.9976	2
Rhy-DC11	1215	250	6.0/0.1	4.62±0.04	0.9980	2
Rhy-DC07-12	1321	950	5.0/0.2	4.73±0.03	0.9996	3
Rhy-DC06-1	1319	1900	4.0/0.2	4.37±0.05	0.9994	3
Rhy-DC06-6	1323	1900	2.3/0.2	4.65±0.03	0.9997	3
Rhy-DC06-7	1629	1900	5.2/0.2	6.47±0.05	0.9994	3
Rhy-DC06-8*	609	1900	2.5/0.2	−5.36±0.07	0.9991	3
Rhy-DC06-9*	407	1900	5.3/0.2	−12.52±0.08	0.9996	3
Rhy-DC06-11	1118	1900	5.1/0.2	2.72±0.05	0.9993	3
Rhy-DC07-14	1120	1900	5.1/0.2	3.05±0.04	0.9996	3

The fitting assumes that $D_{H_2Om}=D_0\exp[(-37.256+75884/T)X]$ where D_0 is to be determined from fits. *: The theoretical profile is convoluted first and then used to fit experimental data (see text). Source of data: (1)=Zhang et al. (1991); (2)=Zhang and Behrens (2000); (3)=this work. Errors for $\ln D_0$ are from least squares fitting and are given at 2σ level.

$\ln A$ on P), the 2σ error would be 1.35, too large to be tolerated. The activation energy (E_a) of D_0 increases from 108±4 kJ/mol at 0.1 MPa to 123±5 kJ/mol at 0.5 GPa to 165±11 kJ/mol at 1.9 GPa.

The extra pressure term in addition to the pressure dependence of the activation energy may be explained in two ways. First, the extra term would result if the activation volume depends on temperature. Starting from (Lasaga, 1998)

$$\ln D = \ln A_0 - \frac{E_0 + P\Delta V_a}{RT}, \tag{8}$$

we have:

$$\ln D = \ln A_0 - \frac{E_0 + P(\Delta V_0 - mRT)}{RT} = \ln A_0 + mP - \frac{E_0 + P\Delta V_0}{RT}, \tag{9}$$

where P is pressure, A_0 is the pre-exponential factor at zero pressure, m is a coefficient, E_0 is the activation energy at zero pressure, and ΔV_a is the activation volume that is expressed as a linear function of temperature. Because the temperature range in H_2O diffusion studies is large (400–1600 °C), the temperature dependence of the activation volume is needed to account for the data. The activation volume for H_2O_m diffusion at low H_2O_t can be calculated from $-RT\partial\ln D_0/\partial P$ using Eq. (7), and is 30±5 cm^3/mol at 0 K and linearly decreases to about 15 cm^3/mol at 965 K and to 0 at 1921 K. In comparison, Nogami and Tomozawa (1984) reported huge activation volume of ~170 cm^3/mol at 465 K and ~72 cm^3/mol at 623 K for water diffusion in silica glass based on diffusion data in a small pressure range (<130 MPa).

Another way to explain the extra pressure term is to utilize the "compensation law" (Winchell, 1969; Lasaga, 1998), which states that $\ln A$ is positively and linearly related to the activation energy. Hence, a dependence of the activation energy on pressure would result in a dependence of $\ln A$ on pressure, as in Eq. (7).

4.2. Diffusivity vs. T, P, and X

In summary, by combining data from this work with that of Zhang et al. (1991) and Zhang and Behrens (2000), molecular H_2O diffusivity may be expressed as follows:

$$D_{H_2O_m} = D_0\exp(aX), \tag{10a}$$

$$\text{with } D_0 = \exp\left(13.375 + 1.8875P - \frac{12939 + 3625.6P}{T}\right), \tag{10b}$$

$$\text{and } a = -37.256 + \frac{75884}{T}. \tag{10c}$$

where T is in K, P is in GPa, D is in $\mu m^2/s$, and X is mole fraction of H_2O_t on a single oxygen basis. From D_{H_2Om} above, total H_2O diffusivity can be obtained as follows (Zhang, 1999b):

$$D_{H_2O_t} = D_{H_2O_m}\frac{dX_m}{dX}, \tag{11a}$$

$$\text{with } \frac{dX_m}{dX} = \frac{16X}{b} - \frac{8X^2}{b^2}\left[8 - 2K + \frac{8K - 2K^2(1-2X) - 16KX}{\sqrt{K^2(1-2X)^2 + 16KX(1-X)}}\right], \tag{11b}$$

$$b = 8X + K(1-2X) + \sqrt{K^2(1-2X)^2 + 16KX(1-X)}, \tag{11c}$$

$$\text{and } K = \exp\left(1.876 - \frac{3110}{T}\right). \tag{11d}$$

This model can be used to calculate H_2O_m and H_2O_t diffusivity from 403–1629 °C, 0–1.9 GPa, and 0.1–7.7 wt.% water content. In order to calculate total H_2O diffusivity using the above procedures, the H_2O_m diffusivity must be used in conjunction with the speciation model of Eq. (11d) (Zhang et al., 1997b), because unlike H_2O_t diffusivity, H_2O_m diffusivity cannot be directly extracted from diffusion profiles and its value depends on the expression of K. Since K at low pressures is used and it may not apply to high pressure, D_{H_2Om} from Eqs. (10a, b, and c) may not be accurate, but D_{H_2Ot} is still accurate as long as self-consistency is maintained. If a new expression of K as a function of temperature and pressure is adopted in the future (Hui et al., 2008a), Eq. (11d) should still be used for calculation of D_{H_2Om} until a new expression of D_{H_2Om} is obtained using new expressions of K.

The dependence of H_2O_t diffusivity on water content, temperature, and pressure is illustrated in Fig. 5. At low water content (<2 wt.%), D_{H_2Ot} is roughly proportional to water content; this dependence becomes exponential as water content is above 2 wt.%. Temperature dependence is always Arrenian, and the activation energy (E_a) increases with pressure and generally decreases with water content. At 1 wt.% H_2O_t, E_a increases from ~81 kJ/mol at 0.1 MPa to ~109 kJ/mol at 0.95 GPa to ~138 kJ/mol at 1.9 GPa; At 5 wt.% H_2O_t, E_a increases from ~46 kJ/mol at 0.1 MPa to ~74 kJ/mol at 0.95 GPa to ~103 kJ/mol at 1.9 GPa. Pressure reduces H_2O diffusion rate, and the negative pressure effect is more noticeable at low temperatures. For example, at 600 °C H_2O_t diffusivity decreases by about one order of magnitude over 1 GPa, whereas at 1200 °C it only decreases by a factor smaller than 2 over the same pressure range.

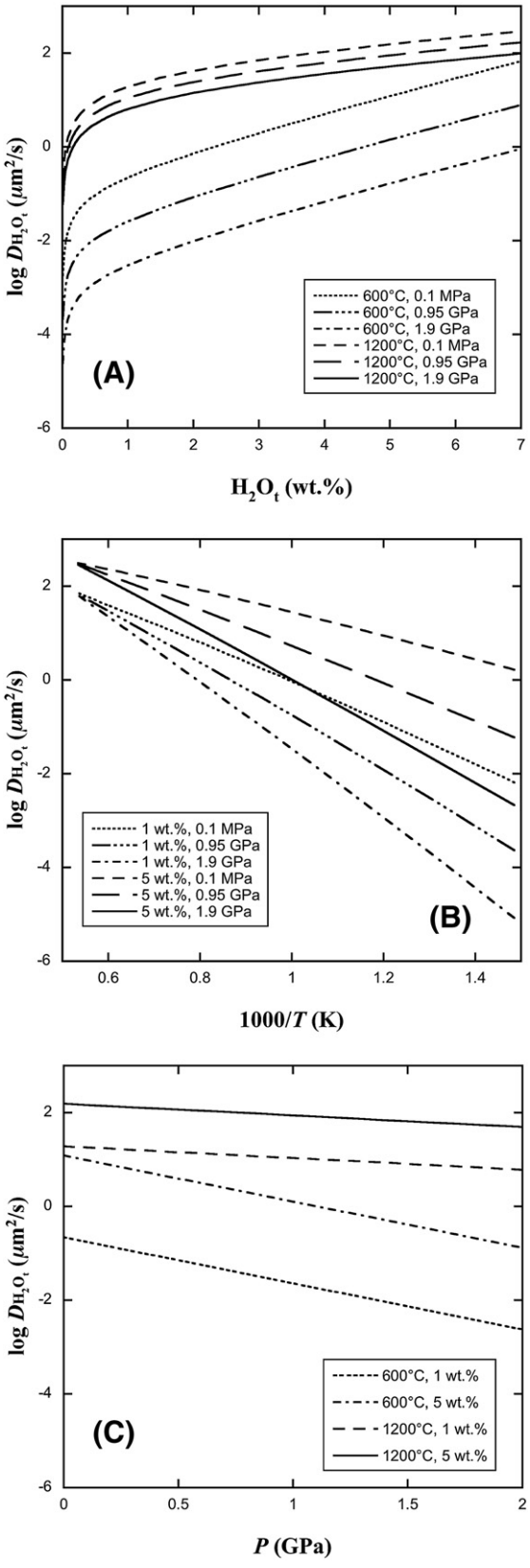

Fig. 5. The dependence of total H_2O diffusivity versus (A) water content, (B) temperature, and (C) pressure, respectively. H_2O_t diffusivity is linear with $1/T$ and P, but it first increases with H_2O_t content proportionally, and then exponentially with the transition at ~2 wt.%.

Because the above procedure to calculate D_{H_2Ot} is fairly complicated, for convenience, the following explicit expression is provided to calculate D_{H_2Ot} (in $\mu m^2/s$):

$$\ln(D_{H_2O_t}/X) = a_0 + a_1X + a_2\sqrt{X} + a_3P - \frac{a_4 + a_5X + a_6\sqrt{X} + a_7P}{T}, \quad (12)$$

with $a_0 = 13.470 \pm 0.035$, $a_1 = -49.996 \pm 0.833$, $a_2 = 7.0827 \pm 0.3524$, $a_3 = 1.8875 \pm 0.0116$, $a_4 = 9532.3 \pm 37.9$, $a_5 = -91933 \pm 913$, $a_6 = 13403 \pm 387$, $a_7 = 3625.6 \pm 12.7$, where X is mole fraction of H_2O_t on a single oxygen basis, T is temperature in K, and P is pressure in GPa. Results from Eq. (12) agree with those from Eqs. (10a) to (11d) within 17%, which is smaller than the experimental error. Furthermore, Eq. (12) is independent of the speciation model.

When H_2O_t content is below 2 wt.%, D_{H_2Ot} is approximately proportional to H_2O_t content, and the following simple equation is obtained for calculating D_{H_2Ot}:

$$D_{H_2O_t} = D^\circ \frac{X}{X_0} = D^\circ \frac{C}{C_0} = \frac{C}{C_0}\exp\left(b_0 + b_1P - \frac{b_2 + b_3P}{T}\right), \quad (13)$$

where $b_0 = 9.5279 \pm 0.0677$, $b_1 = 1.8875 \pm 0.0590$, $b_2 = 9698.5 \pm 74.2$, and $b_3 = 3625.6 \pm 64.7$, C is water content in wt.%, and D° is H_2O_t diffusivity at mole fraction of 0.01789 (X_0) or 1 wt.% (C_0).

4.3. Implication on melt structure

The decrease of H_2O diffusivity with increasing pressure may be explained as follows. Increasing pressure reduces free space in melt structure, and hence reduces the mobility of neutral molecular species such as H_2O_m. This negative pressure effect on diffusivity is consistent with the observation that viscosity of hydrous rhyolite increases with pressure (Hui et al., 2008b). Therefore, hydrous rhyolite behaves like a depolymerized melt, in which diffusion kinetics is slowed by pressure.

Our model results lead to an activation volume of zero at 1648 °C. Above this temperature, H_2O_m diffusivity would increase with increasing pressure. It is not clear whether there is qualitative change in the melt structure leading to a change in the diffusion behavior. Our experimental data have not covered such high temperatures and hence cannot verify the behavior. Such high temperatures are also much higher than normal temperatures of rhyolitic melts.

The activation energy is lowered by increasing water content. This has been observed repeatedly before (e.g., Karsten et al., 1982; Zhang et al., 1991; Zhang and Behrens, 2000; Behrens and Zhang, 2001), and may be attributed to increased porosity with more dissolved water. A lower activation energy at higher H_2O content is also consistent with the observation that H_2O diffusivity increases more rapidly with water content at low temperatures.

4.4. Comparison with other data

In developing the model, some data in the literature was not included. Nowak and Behrens (1997) reported total H_2O diffusivity data at 800–1200 °C, 50–500 MPa, and 0.5–6 wt.% water content also based on diffusion-couple technique. Okumura and Nakashima (2004) investigated H_2O diffusivity <4.1 wt.% at room pressure based on dehydration with *in situ* FTIR. Behrens et al. (2007) studied H_2O diffusivity at 100 MPa from hydration experiments. In particular, Behrens et al. (2007) showed that their data are different from prediction by the model of Zhang and Behrens (2000) by a factor of 2, and attributed the difference to the uncertainty of the pressure effect in the model of Zhang and Behrens (2000). These experimental data are used to evaluate the applicability of our new model.

The comparison between data in Nowak and Behrens (1997) and Behrens et al. (2007) is straightforward. However, Okumura and

Nakashima (2004) reported diffusion-out diffusivity, which is some average of D_{H_2Ot} over a concentration range. To compare their data with D_{H_2Ot} at a given H_2O concentration (the initial and maximum H_2O mole fraction, X_i), a conversion factor must be applied. For the case of proportionality between D_{H_2Ot} and X_i, the correction factor is 0.347 (Wang et al., 1996). For the more general case to higher H_2O concentrations, this factor can be calculated from model profiles at a given temperature, i.e., given parameter of a, equilibrium constant K, and X_i. The mass loss can be found from the model profile of H_2O mole fraction (X) vs. normalized distance $\left(\xi = x/\sqrt{4D_0 t}\right)$ as

$$M = \int_0^{\infty} (X_i - X)\mathrm{d}\xi. \tag{14}$$

It can be derived (Crank, 1975) that the diffusion-out diffusivity D_{out} obtained from mass loss is related to D_0 through

$$\frac{D_{out}}{D_0} = \pi\left(\frac{M}{X_i}\right)^2, \tag{15}$$

Combining Eqs. (4) and (5), D_{H_2Ot} at X_i (D_{X_i}) is related to D_0 through

$$D_{X_i}/D_0 = \exp(aX_i)\cdot(\mathrm{d}X_m/\mathrm{d}X)_{X_i}. \tag{16}$$

Therefore we find the conversion factor as

$$D_{out}/D_{X_i} = \frac{\pi M^2}{X_i^2 \cdot \exp(aX_i)\cdot(\mathrm{d}X_m/\mathrm{d}X)_{X_i}}. \tag{17}$$

The conversion factor thus obtained depends somewhat on temperature, and is ~0.324 for 0.7 wt.%, 0.207–0.243 for 1.9 wt.%, and 0.146–0.198 for 2.8 wt.% H_2O_t, for the temperature range of Okumura and Nakashima (2004). Their H_2O_t diffusivities at 4.1 wt.% are not included in the comparison because they are similar to or even smaller than those at 2.8 wt.% at the same temperature, which is against the observed general trend of H_2O diffusivity.

Fig. 6 compares these experimental data and calculations based on our model, indicating good inter-laboratory and multi-method consistency and therefore demonstrating the reliability of our model. The maximum difference is a factor of 2.3 between our calculation and D_{H_2Ot} of Nowak and Behrens (1997) using the Boltzmann–Matano method. Such a difference is expected because the precision of the Boltzmann–Matano method is not high. H_2O_t diffusivities at 1 wt.% H_2O_t from Behrens et al. (2007) are within a factor of 1.3, and those at 4 wt.% H_2O_t from Behrens et al. (2007) are within a factor of 1.6 with those predicted by our model. The differences are only slightly larger than the experimental and model uncertainty, and may be attributed to complications in hydration experiments (such as dissolution during the experiment and precipitation during quench). Resolving the pressure effect on H_2O diffusion is the main goal of this study. The good agreement between our new H_2O diffusion model and previous experimental data including those of Behrens et al. (2007) suggests that the pressure effect is now resolved well.

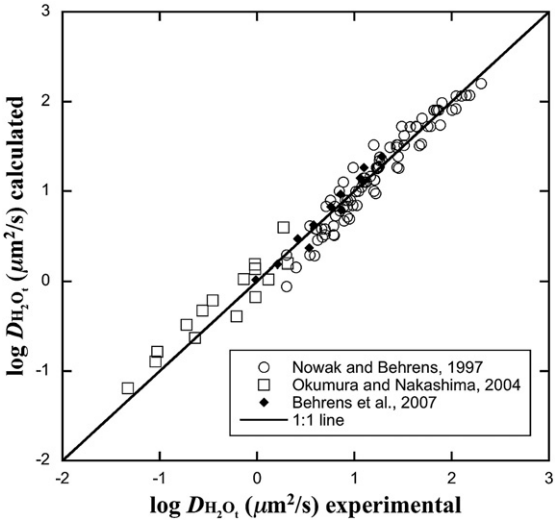

Fig. 6. Comparison between our new diffusivity expression and experimental data in three papers: Nowak and Behrens (1997); Okumura and Nakashima (2004); and Behrens et al. (2007). The diffusion-out diffusivity of Okumura and Nakashima (2004) is converted to D_{H_2Ot} (the data point at 500 °C and 0.7 wt.% H_2O_t is not included due to species disequilibrium, Zhang et al., 2007). See text for details.

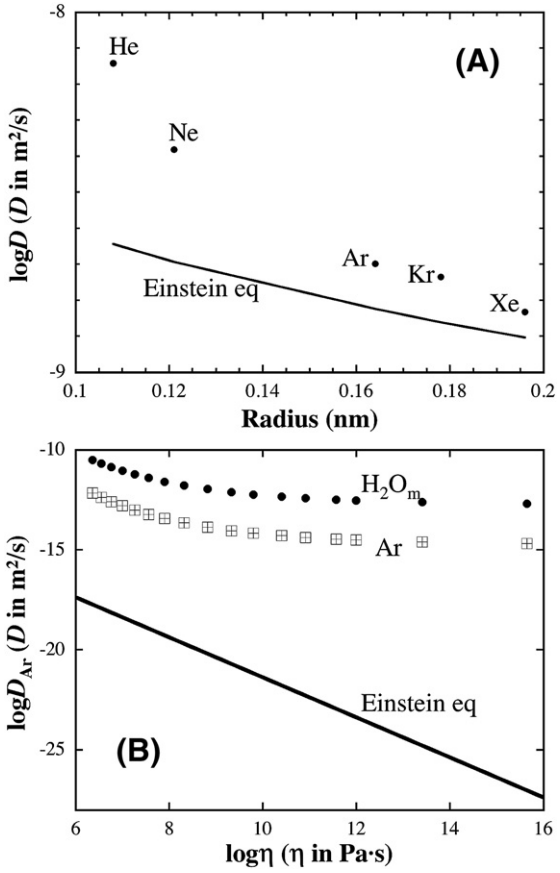

Fig. 7. (A) Noble gas diffusivity in water versus radius, and (B) H_2O_m and Ar diffusivity in rhyolitic melt versus viscosity of the melt at 600 °C and 0.1–6.0 wt.% H_2O_t. Note the vertical scale difference in (A) and (B). Molecular H_2O diffusion data are from this study. Ar diffusion data are from Behrens and Zhang (2001). Viscosity of rhyolitic melts is from Zhang et al. (2003). Atomic radii of molecular H_2O and Ar are taken to be 0.137 nm and 0.164 nm respectively (Shannon, 1976; Zhang and Xu, 1995). The calculated Einstein diffusivity (solid line) for H_2O_m and Ar in rhyolitic melt are similar at this scale.

4.5. Applicability of the Einstein or Eyring equation to molecular H_2O diffusion

The Einstein (1905) equation relates diffusivity of a neutral species in a liquid and the viscosity of the liquid, and is derived by considering molecular diffusion as Brownian motion in the liquid continuum. It takes the following form:

$$D = kT/(\eta L), \tag{18}$$

where D is diffusivity, k is the Boltzmann constant, T is temperature in K, η is viscosity, and L is a length scale and equals $6\pi r$ where r is the radius of the diffusing species. The equation can predict the diffusivity of Ar, Kr and Xe in water to within 30% (Jahne et al., 1987; Fig. 7A). It does not seem that the relation has been applied to silicate melts.

Fig. 7B compares experimental diffusivity of molecular H_2O and Ar with the calculated Einstein diffusivity. The latter is smaller than the

experimental data by many orders of magnitude. Because the uncertainty in the diffusivities is less than a factor of 2, and that in the viscosities is less than a factor of 3, these uncertainties cannot explain the huge discrepancy of the Einstein equation. Therefore, the Einstein equation cannot predict diffusivity of molecular H_2O and Ar in rhyolitic melt. Not only do the values not match, but also the slope of log$D$ versus logη is not −1. Furthermore, the slope is not even a constant (i.e., log$D$ versus logη is not linear)! The failure of the Einstein equation is likely due to the large size of ionic clusters (such as SiO_4^{4-}, $Si_2O_7^{6-}$, etc.) in silicate melts, which are larger than molecular H_2O or Ar, meaning that the motion of the molecules in the melt cannot be treated as large molecules moving through a liquid continuum.

The Eyring equation (Glasstone et al., 1941) is based on the transition state theory and assumes that the diffusion and viscous flow involve the same process. The equation has been shown to work for ^{18}O and ^{30}Si diffusion in some silicate melts (e.g., Shimizu and Kushiro, 1984; Lesher et al., 1996; Tinker and Lesher, 2001; Reid et al., 2003; Tinker et al., 2004), but does not work for, e.g., ^{18}O diffusion in hydrous rhyolitic melt (Behrens et al., 2007). It takes the same form as Eq. (18), but L is the jumping distance, which is often taken to be the diameter of the diffusing species. Hence, the difference between the Eyring equation and the Einstein equation is about a factor of 10. As can be seen from Fig. 7B, a factor of 10 (or one order of magnitude) is not enough to reconcile the experimental and calculated diffusivities. Hence, the Eyring equation does not work here, which is expected because the process for viscous flow involves motion of the aluminosilicate network, but that of Ar and H_2O_m diffusion does not.

5. Conclusions

Water diffusion in rhyolite at 0.95–1.9 GPa and 407–1629 °C is investigated to constrain the pressure dependence of H_2O diffusivity. High pressure results in a smaller diffusivity, which is attributed to decreased free space in the melt. This negative pressure effect indicates that the process of magma upwelling facilitates bubble growth not only thermodynamically (by reducing H_2O solubility), but also kinetically (by increasing H_2O diffusivity), although the latter effect is smaller. Based on a model that H_2O_m dominates water diffusion, two specific H_2O_t diffusivity expressions have been constructed: one for both low and high total H_2O contents (up to 7.7 wt.%), and the other simple form is applicable to low H_2O contents (up to 2 wt.%). All of the expressions are only applicable when species equilibrium is roughly maintained (Jambon et al., 1992), meaning relatively high temperatures and high H_2O_t contents. For example, at 500 °C, H_2O_t needs to be ≥1 wt.% for the diffusivities to be applicable. With this study, we have resolved the pressure effect on H_2O diffusion in rhyolitic melt so that H_2O diffusivity can be predicted from 0 to 2 GPa and from 400 to 1600 °C. We recommend the use of these expressions in modeling bubble growth in and degassing from a rhyolitic melt, and the dynamics of H_2O-driven explosive rhyolitic eruptions, as well as H_2O transport in granitic magma chambers.

Acknowledgments

We thank Hejiu Hui and Harald Behrens for providing hydrous rhyolite glasses, Zhengjiu Xu for training in the lab, Yang Chen on electron microprobe analyses, Yan Liang and Eric Essene for insightful and constructive comments, and Rebecca Lange, Sam Mukasa, and Zhan Chen for discussion. This work is supported by NSF grants (EAR-0228752, -0537598, -0711050).

References

Bartholomew, R.F., Schreurs, J.W.H., 1980. Wide-line NMR study of protons in hydrosilicate glasses of different water content. J. Non-Cryst. Solids 38&39, 679–684.

Behrens, H., Nowak, M., 1997. The mechanisms of water diffusion in polymerized silicate melts. Contrib. Mineral. Petrol. 126, 377–385.

Behrens, H., Zhang, Y., 2001. Ar diffusion in hydrous silicic melts: implications for volatile diffusion mechanisms and fractionation. Earth Planet. Sci. Lett. 192, 363–376.

Behrens, H., Zhang, Y., Xu, Z., 2004. H_2O diffusion in dacitic and andesitic melts. Geochim. Cosmochim. Acta 68, 5139–5150.

Behrens, H., Zhang, Y., Leschik, M., Wiedenbeck, M., Heide, G., Frischat, G.H., 2007. Molecular H_2O as carrier for oxygen diffusion in hydrous silicate melts. Earth Planet. Sci. Lett. 254, 69–76.

Bose, K., Ganguly, J., 1995. Quartz–coesite transition revisited: reversed experimental determination at 500–1200 °C and retrieved thermochemical properties. Am. Mineral. 80, 231–238.

Crank, J., 1975. The Mathematics of Diffusion. Oxford University Press. 414 pp.

Delaney, J.R., Karsten, J.L., 1981. Ion microprobe studies of water in silicate melts: concentration-dependent water diffusion in obsidian. Earth Planet. Sci. Lett. 52, 191–202.

Einstein, A., 1905. The motion of small particles suspended in static liquids required by the molecular kinetic theory of heat. Ann. Phys. 17, 549–560 (in German).

Freda, C., Baker, D.R., Romano, C., Scarlato, P., 2003. Water diffusion in natural potassic melts. Geol. Soc. Spec. Publ. 213, 53–62.

Friedman, I., Long, W., 1976. Hydration rate of obsidian. Science 191, 347–352.

Ganguly, J., Bhattacharya, R.N., Chakraborty, S., 1988. Convolution effect in the determination of compositional profiles and diffusion coefficients by microprobe step scans. Am. Mineral. 73, 901–909.

Glasstone, S., Laidler, K.J., Eyring, H., 1941. The Theory of Rate Processes. McGraw-Hill, New York. 611 pp.

Hui, H., Zhang, Y., Xu, Z., Behrens, H., 2008a. Pressure dependence of the speciation of dissolved H_2O in rhyolitic melt. Geochim. Cosmochim. Acta in revision.

Hui, H., Zhang, Y., Xu, Z., Gaudio, P.D., Behrens, H., 2008b. Pressure dependence of viscosity of rhyolitic melts. Geochim. Cosmochim. Acta submitted.

Jahne, B., Heinz, G., Dietrich, W., 1987. Measurement of the diffusion coefficients of sparingly soluble gases in water. J. Geophys. Res. C92, 10767–10776.

Jambon, A., 1979. Diffusion of Water in a Granitic Melt: An Experimental Study. Yearbook. Carnegie Inst., Washington, pp. 352–355.

Jambon, A., Zhang, Y., Stolper, E.M., 1992. Experimental dehydration of natural obsidian and estimation of D_{H_2O} at low water contents. Geochim. Cosmochim. Acta 56, 2931–2935.

Karsten, J.L., Holloway, J.R., Delaney, J.R., 1982. Ion microprobe studies of water in silicate melts: temperature-dependent water diffusion in obsidian. Earth. Planet. Sci. Lett. 59, 420–428.

Lapham, K.E., Holloway, J.R., Delaney, J.R., 1984. Diffusion of H_2O and D_2O in obsidian at elevated temperatures and pressures. J. Non-Cryst. Solids 67, 179–191.

Lasaga, A.C., 1998. Kinetic Theory in the Earth Sciences. Princeton University Press.

Lesher, C.E., Hervig, R.L., Tinker, D., 1996. Self diffusion of network formers (silicon and oxygen) in naturally occurring basaltic liquid. Geochim. Cosmochim. Acta 60, 405–413.

Liu, Y., Zhang, Y., 2000. Bubble growth in rhyolitic melt. Earth Planet. Sci. Lett. 181, 251–264.

Liu, Y., Zhang, Y., Behrens, H., 2004. H_2O diffusion in dacitic melts. Chem. Geol. 209, 327–340.

Newman, S., Stolper, E.M., Epstein, S., 1986. Measurement of water in rhyolitic glasses: calibration of an infrared spectroscopic technique. Am. Mineral. 71, 1527–1541.

Nogami, M., Tomozawa, M., 1984. Effect of stress on water diffusion in silica glass. J. Am. Ceram. Soc. 67, 151–154.

Nowak, M., Behrens, H., 1997. An experimental investigation on diffusion of water in haplogranitic melts. Contrib. Mineral. Petrol. 126, 365–376.

Okumura, S., Nakashima, S., 2004. Water diffusivity in rhyolitic glasses as determined by in situ IR spectrometry. Phys. Chem. Miner. 31, 183–189.

Okumura, S., Nakashima, S., 2006. Water diffusion in basaltic to dacitic glasses. Chem. Geol. 227, 70–82.

Orlova, G.P., 1962. The solubility of water in albite melts. Int. Geol. Rev. 6, 254–258.

Press, W.H., Teukolsky, S.A., Vetterling, W.T., Flannery, B.P., 1992. Numerical Recipes in Fortran 77: The Art of Scientific Computing, 2nd Ed. Cambridge University Press, New York.

Reid, J.E., Suzuki, A., Funakoshi, K., Terasaki, H., Poe, B.T., Rubie, D.C., Ohtani, E., 2003. The viscosity of $CaMgSi_2O_6$ liquid at pressures up to 13 GPa. Phys. Earth Planet. Inter. 139, 45–54.

Shannon, R.D., 1976. Revised effective ionic radii and systematic studies of interatomic distances in halides and chalcogenides. Acta Crystallogr. A32, 751–767.

Shaw, H.R., 1974. Diffusion of H_2O in granitic liquids: I. Experimental data; II. Mass transfer in magma chambers. In: Hofmann, A.W., Giletti, B.J., Yoder, H.S., Yund, R.A. (Eds.), Geochemical Transport and Kinetics. Carnegie Inst. Washington Publ., Washington, DC, pp. 139–170.

Shimizu, N., Kushiro, I., 1984. Diffusivity of oxygen in jadeite and diopside melts at high pressures. Geochim. Cosmochim. Acta 48, 1295–1303.

Stolper, E.M., 1982. Water in silicate glasses: an infrared spectroscopic study. Contrib. Mineral. Petrol. 81, 1–17.

Tinker, D., Lesher, C.E., 2001. Self diffusion of Si and O in dacitic liquid at high pressures. Am. Mineral. 86, 1–13.

Tinker, D., Lesher, C.E., Baxter, G.M., Uchida, T., Wang, Y., 2004. High-pressure viscometry of polymerized silicate melts and limitations of the Eyring equation. Am. Mineral. 89, 1701–1708.

Wang, L., Zhang, Y., Essene, E.J., 1996. Diffusion of the hydrous component in pyrope. Am. Mineral. 81, 706–718.

Wasserburg, G.J., 1988. Diffusion of water in silicate melts. J. Geol. 96, 363–367.

Watson, E.M., 1991. Diffusion of dissolved CO_2 and Cl in hydrous silicic to intermediate magmas. Geochim. Cosmochim. Acta 55, 1897–1902.
Winchell, P., 1969. The compensation law for diffusion in silicates. High Temp. Sci. 1, 200–215.
Withers, A.C., Behrens, H., 1999. Temperature-induced changes in the NIR spectra of hydrous albitic and rhyolitic glasses between 300 and 100 K. Phys. Chem. Minerals 27, 119–132.
Withers, A.C., Zhang, Y., Behrens, H., 1999. Reconciliation of experimental results on H_2O speciation in rhyolitic glass using in-situ and quenching techniques. Earth Planet. Sci. Lett. 173, 343–349.
Zhang, Y., 1999a. A criterion for the fragmentation of bubbly magma based on brittle failure theory. Nature 402, 648–650.
Zhang, Y., 1999b. H_2O in rhyolitic glasses and melts: measurement, speciation, solubility, and diffusion. Rev. Geophys. 37, 493–516.
Zhang, Y., Stolper, E.M., 1991. Water diffusion in basaltic melts. Nature 351, 306–309.
Zhang, Y., Xu, Z., 1995. Atomic radii of noble gas elements in condensed phases. Am. Mineral. 80, 670–675.
Zhang, Y., Behrens, H., 2000. H_2O diffusion in rhyolitic melts and glasses. Chem. Geol. 169, 243–262.
Zhang, Y., Stolper, E.M., Wasserburg, G.J., 1991. Diffusion of water in rhyolitic glasses. Geochim. Cosmochim. Acta 55, 441–456.
Zhang, Y., Stolper, E.M., Ihinger, P.D., 1995. Kinetics of the reaction $H_2O+O=2OH$ in rhyolitic and albitic glasses: preliminary results. Am. Mineral. 80, 593–612.
Zhang, Y., Jenkins, J., Xu, Z., 1997a. Kinetics of the reaction $H_2O+O=2OH$ in rhyolitic glasses upon cooling: geospeedometry and comparison with glass transition. Geochim. Cosmochim. Acta 61, 2167–2173.
Zhang, Y., Belcher, R., Ihinger, P.D., Wang, L., Xu, Z., Newman, S., 1997b. New calibration of infrared measurement of dissolved water in rhyolitic glasses. Geochim. Cosmochim. Acta 61, 3089–3100.
Zhang, Y., Xu, Z., Behrens, H., 2000. Hydrous species geospeedometer in rhyolite: improved calibration and application. Geochim. Cosmochim. Acta 64, 3347–3355.
Zhang, Y., Xu, Z., Liu, Y., 2003. Viscosity of hydrous rhyolitic melts inferred from kinetic experiments, and a new viscosity model. Am. Mineral. 88, 1741–1752.
Zhang, Y., Xu, Z., Zhu, M., Wang, H., 2007. Silicate melt properties and volcanic eruptions. Rev. Geophys. 45, RG4004. doi:10.1029/2006RG000216.